Hindawi
Advances in Civil Engineering
Volume 2019, Article ID 1482736, 14 pages
https://doi.org/10.1155/2019/1482736

Research Article

Analysis of the Seismic Demand of High-Performance Buckling-Restrained Braces under a Strong Earthquake and Its Aftershocks

Luqi Xie,[1] Jing Wu,[1] Qing Huang,[2] and Chao Tong[1]

[1]*Key Laboratory on Concrete and Prestressed Concrete Structures of Ministry of Education, Southeast University, Nanjing 210096, China*
[2]*Architects & Engineers Co., Ltd. of Southeast University, Nanjing 210096, China*

Correspondence should be addressed to Jing Wu; seuwj@seu.edu.cn

Received 15 November 2018; Accepted 9 January 2019; Published 6 February 2019

Academic Editor: Raffaele Landolfo

The analysis of the ductility and cumulative plastic deformation (CPD) demand of a high-performance buckling-restrained brace (HPBRB) under a strong earthquake and its aftershocks is conducted in this paper. A combination of three continuous excitations with the same ground motion is used to simulate the affection of a strong earthquake and its aftershocks. A six-story HPBRB frame (HPBRBF) is taken as an example to conduct the incremental dynamic analysis (IDA). The seismic responses of the HPBRBF under one, two, and three constant continuous ground motions are compared. The IDA result indicates that the ductility and CPD demand of the BRBs under the three constant continuous ground motions are significantly larger than that excited by only one. Probabilistic seismic demand analysis (PSDA) is performed using seven near-fault ground motions and seven far-fault ground motions to consider the indeterminacy of ground motion. The probabilistic seismic demand curves (PSDCs) for the ductility and CPD demand for the HPBRB under the strong earthquake and its aftershocks are obtained in combining the probabilistic seismic hazard analysis. The results indicate that the AISC threshold value of the CPD with 200 is excessively low for a HPBRBF which suffers the continuous strong aftershocks with near-fault excitations, and a stricter threshold value should be suggested to ensure the ductility and plastic deformation capacity demand of the HPBRB.

1. Introduction

A buckling-restrained brace (BRB; Figure 1) is a type of metal-yield energy dissipation device, which can be fabricated in a frame structure as a brace to provide lateral stiffness during the lifetime of the structure. If the frame suffers a strong earthquake, the BRB will yield before the main structural members and dissipate the seismic energy, protecting the main structural members from severe damage [1]. The BRB could be used as a brace and damper in newly built structures, as well as a seismic retrofitting measure to existing structures [2]. The BRBs on structures in high seismic zones tend to experience high-strain cyclic deformation under strong earthquakes and aftershocks, and high-strain low-cycle fatigue failure may occur on the BRBs after several large-strain cycles. The seismic capacity of a structure largely depends on the low-cycle fatigue property of the BRBs [3, 4], which is closely related to the ductility (μ) and the cumulative plastic deformation (CPD) of the BRB, expressed as follows:

$$\mu = \max \frac{\left(\varepsilon_{\text{tmax}}, \left|\varepsilon_{\text{cmax}}\right|\right)}{\varepsilon_{\text{y}}},$$
$$\text{CPD} = \sum \frac{\left|\Delta\varepsilon_{pi}\right|}{\varepsilon_{\text{y}}}, \tag{1}$$

where $\varepsilon_{\text{tmax}}$ is the maximum tensile strain of the BRB, $\varepsilon_{\text{cmax}}$ is the maximum compressive strain, $\Delta\varepsilon_{pi}$ is the strain amplitude of the i^{th} cycle, and ε_{y} is the yield strain of the BRB.

Figure 1: A BRB frame (a library in the USA).

Researchers have performed extensive studies on the BRB frame (BRBF) to measure the demand of the energy dissipation capacity of the BRB, and studies on the low-cycle fatigue property of BRBs in a single ground motion have been relatively fully developed. FEMA-450 [5] comments the CPD demand of a BRB no less than 140 through experimental studies and nonlinear time-history analyses. Sabelli [6] proposed that the demand should reach 185 based on the time-history analyses on a three-story and a six-story BRBF. Iwata et al. [7] suggested that the CPD should reach 292, while Usami et al. [8] proposed the CPD capacity no less than 400. ANSI/AISC [9] stipulates that the CPD of the BRB should be at least 200 to ensure the requirement of the low-cycle fatigue property.

BRBs that fulfill the above CPD requirement are supposed to help the frames resist one strong ground motion, while it should be replaced in time after a strong earthquake to restore the capacity of the structures. However, the existed research about earthquake records indicate that strong earthquakes often arise with several strong aftershocks [10], and the interval between the shocks is too short to replace the BRBs. Furthermore, aftershocks may cause further damage accumulation, which leads to the failure of the BRB and results in the collapse of the frame structure, especially for near-fault ground motions. To resist the strong aftershocks, the demand of the ductility and the CPD should be raised. Usami et al. [11] proposed the high-performance BRB (HPBRB), in which the special performance requirements can be summarized as follows: (1) stable hysteretic characteristics and high energy dissipation capacity; (2) high deformation capacity; (3) high low-cycle fatigue strength; (4) easy and low-cost fabrication and construction; (5) high durability; and (6) no need for replacement under continuous strong earthquakes. It is concluded that a high low-cycle fatigue capacity is needed to ensure the energy dissipation capacity of the BRB by selecting high-ductility steel. Researchers proposed a series of novel HPBRBs, which was based on the construction of the specimens and the material specimens. Jia et al. [12] proposed an assembled buckling-restrained brace wrapped with carbon or basalt fiber, which could improve the restraining members and sufficient ductility and energy dissipation capacity. Jia et al. [13] proposed a type of fish-bone BRB (FB-BRB), which could avoid strain concentration along the length of the core member and improve the energy dissipation capacity during a strong earthquake or subsequent repeated aftershocks. Wang et al. [14] proposed a novel BRB with partial buckling restraint, in which only the edge parts of the core member are strained and other parts are designed for visual inspection on damage monitoring. Chen et al. [15] experimentally studied on the effect of the unbonding materials on the mechanic behavior of all-steel BRBs and suggested that the unbonding materials should be applied for high-performance BRBs with a relatively long yielding segment and thin core plate. Guo et al. [16–19] proposed a series of high-performance BRBs, such as shuttle-shaped BRBs [16], cross-arm pretensioned cable stayed BRBs [17, 18], and corrugated-web-connected BRBs [19]. Xie et al. [20] proposed a type of weld-free all-steel BRBs, in which the core member is fabricated absolutely in high-strength bolts without any weld, and a high CPD could be seen in the low-cycle fatigue tests. Besides, Hoveidae et al. [21] numerically studied the seismic behavior of short-core all-steel BRB (SCBRB), in which the relationship between the ductility demand and the core length was analyzed. Vafaei and Eskandari [22] studied on the seismic response of BRBs subjected to the fling step and forward directivity near-fault ground motions and confirmed that the near-fault ground motions imposed higher demands on the structures. However, a unified demand for the ductility and CPD of a BRB under the action of a strong earthquake and its aftershocks has not been unified yet.

In this paper, the distribution characteristics of ductility and CPD of BRBs are determined by the incremental dynamic analysis (IDA) [23] using three continuous equal-intensity earthquake ground motions to consider the effect of an earthquake and its aftershocks. As it is essential to analyze the randomness of the response by the probability method, the seismic demand of the ductility and CPD of the BRB are concluded through the probability seismic demand analysis (PSDA) [24]. The seismic demand index of μ and CPD of the HPBRB is also suggested in this paper, which could be used as a threshold value criterion for manufacturing HPBRB.

2. Application of PSDA in HPBRB Design

According to the theory proposed by the PEER, the seismic response of a structure is described as the engineering demand parameter (EDP), and the peak ground acceleration (PGA) of the ground motion is chosen as the intensity measure (IM) in this paper, while the considered period of time is determined as 50 years according to the design reference period of the common engineering structures in China. When the probabilistic seismic hazard curve (PSHC) of the PGA under the condition of a given site is combined with the probability distribution of the EDP under the given PGA, the probability of the EDP of the structure exceeding a certain value in 50 years can be obtained.

The probabilistic seismic demand, $\lambda_{\mathrm{EDP}}(\delta)$, which is the probability of the EDP exceeding a certain value δ in 50 years, can be divided into two parts: one part is the

conditional probability of exceeding the demand value δ under the condition PGA = A. The other is the probability of PGA of the ground motion around the value A. The formula of probabilistic seismic demand can be expressed as

$$\lambda_{\mathrm{EDP}}(\delta) = \int_A P[\mathrm{EDP} > \delta \mid \mathrm{PGA} = A] \cdot \left| d\lambda_{\mathrm{PGA}}(A) \right|, \quad (2)$$

where $P[\mathrm{EDP} > \delta \mid \mathrm{PGA} = A]$ is the probability of exceeding a specified EDP level δ, given as a level of PGA = A. The differential of the ground motion hazard curve, $d\lambda_{\mathrm{PGA}}(A) = \lambda_{\mathrm{PGA}}(A) - \lambda_{\mathrm{PGA}}(A + dA)$, is the probability that the value of PGA belongs to $(A, A + dA)$ in 50 years, where dA is a small increment in PGA.

Incremental dynamic analysis (IDA) is conducted in this paper to obtain the accurately seismic responses of the HPBRB frame (HPBRBF) under different levels of ground motion intensity, which is an essential step in PSDA. The essence of IDA in this paper is scaling the PGA of one ground motion into several different levels to form a series of ground motions. Then, the nonlinear dynamic time-history analyses on the HPBRBF are conducted based on each ground motion, and the IDA curves which can reveal the relationships between the EDP of the HPBRBF and the PGA of the ground motions are obtained. Furthermore, a series of seismic recording should be selected to conduct the IDA, and the statistical analysis of the seismic demand curves of IDA considering the randomness of the earthquake is essential.

The analysis steps of PSDA are as follows:

(1) Establish the computational model of the HPBRBF

(2) Select the seismic records and determine the PGA

(3) Select the appropriate parameters of the EDP and conduct IDA

(4) Conduct statistical analysis of the seismic demand curves of IDA along with the probability distribution of seismic demand parameters and calculate the probability of the EDP exceeding a certain value demand under a specified PGA

(5) Obtain the probability seismic hazard curves (PSHCs) of the PGA under certain conditions

(6) Establish the probability seismic demand curves (PSDCs) according to the conditional probability of the seismic demand under the specified PGA and its PSHC

As the main performance indexes of a BRB are ductility and CPD, they are chosen as the EDPs when conducting PSDA for an HPBRB. Based on considering the randomness of the intensity and frequency of earthquakes and their aftershocks, the IDA is conducted to obtain the PSDC of the HPBRBs on the frame. Combined with the PSHC of specific site conditions, the PSDC of the HPBRB can be obtained through the probability method, including the PSDC of ductility and CPD.

3. Model of HPBRBF and Ground Motions

The HPBRB frame (HPBRBF) model is chosen as a six-story office building composed of a steel frame and Chevron HPBRBs [25]. The height of the story is 3.9 m, and the span of the frame is 8.0 m. The base of the column is fully restrained on the ground. The elevation of the frame is shown in Figure 2. According to the Code of Seismic Design of Buildings in China (GB50011-2010) [26], the building is designed in a zone whose seismic precautionary intensity is 8°, the character of the site belongs to Type III, and the design characteristic period of ground motion belongs to the first group. The seismic precautionary intensity is stipulated by "Standard for classification of seismic protection of building construction (GB50223-2008)" in China. The seismic precautionary intensity stands for the seismic intensity whose exceedance probability is 10% in 50 years, while 8° stands for the fortification acceleration is 2.0 m/s^2. The nominal values of the dead load and the live load are 6.0 kN/m^2 and 3.0 kN/m^2, respectively. The uniformly distributed loads are simplified into a series of concentrated loads on the nodes of beam elements of the structure.

The steel frame is composed of welded H-section beams and box-section columns. The beams are fixed with the columns. In addition, the BRBs are jointed with the frame. It is assumed that the yield stress of steel (f_y) for both beams and columns is 345 MPa, while that for the BRB is 235 MPa. Young's modulus (E_s) and Poisson's ratio of the steel are 206,000 N/mm^2 and 0.3, respectively. The density of steel is 7,850 kg/m^3. The section parameters of the members on the HPBRBF are shown in Table 1.

Nonlinear dynamic time history analysis is performed by SeismoStruct (SeismoSoft [27]). The beams and columns of the frame are modelled as the load-based inelastic fiber space frame beam-column element (infrmFB). The load-displacement relation of the beams and the columns can be obtained by integrating the nonlinear uniaxial stress-strain relations of the entire fibers on the sections of the infrmFBs under the plane-section assumption. The HPBRBs are modelled as the nonlinear truss elements, which can only bear axial force. The axial elastic stiffness of the elements is determined by the material model and the section parameters. Since the HPBRBs installed in the frame with connection parts and transition parts at two ends would occupy some geometric dimension in actual engineering, the length of an HPBRB yielding segment is assumed as only about half of the geometric element length used in the model [28]. As the strain of the BRB should be calculated as the ratio between the deformation and the length of the yielding segment, the simplified numerical model of BRB in this study assumed that the full length of the member is arranged as the yielding segment, and the result of the analysis model should be multiplied by 2 in the postprocessing process to obtain the ductility and the CPD of the HPBRB in the actual structure. A bilinear stress-strain relation with $E_t = E_s/100$ (where E_t is the tangent modulus after yield) and a kinematic hardening rule are adopted for the steel beams and columns, while $E_t = E/60$ for the HPBRB members in the time-history analysis according to Usami et al. [28]. Owing to the complexity of the beam element modelling, a simplified model for BRBs is then considered, which models the BRB with a truss element using a bilinear stress-strain relationship with a kinematic hardening rule. According to Usami

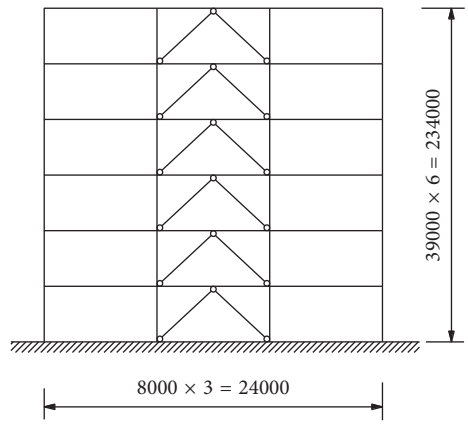

Figure 2: Elevation of the frame.

Table 1: Member section of the beam, column, and BRBs of the six-story HPBRBF.

Story	SC (mm) □ $C \times t$	IC (mm) □ $C \times t$	SB (mm) H · $h \times b \times t_w \times t_f$	MB (mm) H · $h \times b \times t_w \times t_f$	A_{BRB} (mm^2)
1-2	390×15	510×27	$450 \times 200 \times 10 \times 16$	$500 \times 250 \times 12 \times 20$	3731
3-4	370×13	440×16	$450 \times 200 \times 10 \times 16$	$500 \times 250 \times 12 \times 20$	3142
5-6	330×11	400×14	$450 \times 200 \times 10 \times 16$	$500 \times 250 \times 12 \times 20$	2281

Note. SC is the dimensions of the side columns; IC is the dimensions of the inner columns; SB is the dimensions of the side beams; MB is the dimensions of the middle beams; A_{BRB} is the sectional area of HPBRBs. The symbol "□" represents the square steel pipe, which could be regarded as the box-section columns.

et al. [28], the truss model with a strain hardening stiffness of $E_s/60$ exhibits close energy dissipation capacity to the beam element modelling result, and thus, it is believed to be appropriate for modelling the BRBs. Therefore, the truss model with the bilinear constitutive model is applied to BRBs in the analysis of the present study. The period of vibration of the selected model is 0.980 s.

It is worth mentioning that the value of A_{BRB} in Table 1 is referred to the yielding core. The stiffness and the strength of the BRB is mainly affected by that of the yielding segment in the postyielding stage according to the theory of stiffness in series of the core member, which could be expressed as

$$K_{BRB} = \frac{1}{\left((1/K_i) + (2/K_{con}) + (2/K_{tr})\right)}, \quad (3)$$

where $K_i = EA_i/L_i$ is the stiffness of the yielding segment, while $K_{con} = EA_{con}/L_{con}$ and $K_{tr} = EA_{tr}/L_{tr}$ are the stiffness of connection and transition segments of the BRB. A_i, A_{con}, and A_{tr} refers to the sectional area of the yielding segment, transition segment, and connection segment, respectively; while L_i, L_{con}, and L_{tr} are the length of the three segments. As E is Young's modulus of Q235 steel, it should be replaced as E_t which is the tangent modulus in the postyielding stage. Because only the yielding segment yields during the earthquake, the postyielding stiffness of the BRB mainly depends on that of the yielding segment. Besides, the strength of BRB is determined by the minimum sectional area of the whole brace, and thus, the simplified model could replicate the stiffness and strength properly.

It can be concluded from the existed ground motion records that the near-fault ground motions with velocity pulse may cause a relatively large peak ground velocity (PGV) and PGA. The near-fault ground motions will make a wide acceleration sensitive region which may significantly affect the structural response, and this effect would significantly increase the roof-displacement, interstory drift, and the demand of the base shear force of the HPBRBF. Kalkan and Kunnath [29] proposed that the near-fault should be defined as fault distance less than 20 km as well as PGV/PGA > 0.2. In this study, seven near-fault ground motions whose fault distances are within 15 km with PGV/PGA > 0.2 are selected from the PEER ground motion database considering the duration, the magnitude, the epicenter distance, and the site condition of the ground motion, along with the magnitude of all the selected records greater than 6.0. Besides, seven far-fault ground motions are selected from the PEER ground motion database according to the principal that the deviation of the mean accelerogram spectrum from the target spectrum is minimum [30], as is shown in Figure 3. The target spectrum is selected according to "Code for seismic design of buildings (GB50011-2010)" in China, in which the seismic precautionary intensity is 8°, as is shown in Figure 3. The mean spectrum of the selected ground motions is also shown in the figure, in which the deviations between the mean spectrum and target spectrum is minimum between the period 0.8 s to 1.0 s. As the period of vibration of the selected model is 0.980 s, the ground motion records could be used.

The parameters of the ground motion records are shown in Tables 2 and 3, in which the PGV and the PGA are listed. The site types in the table are classified according to the USGS classification criteria of the United States, which is close to the Type III site specified in the Code for Seismic Design of Buildings in China (GB50011-2010). It should be

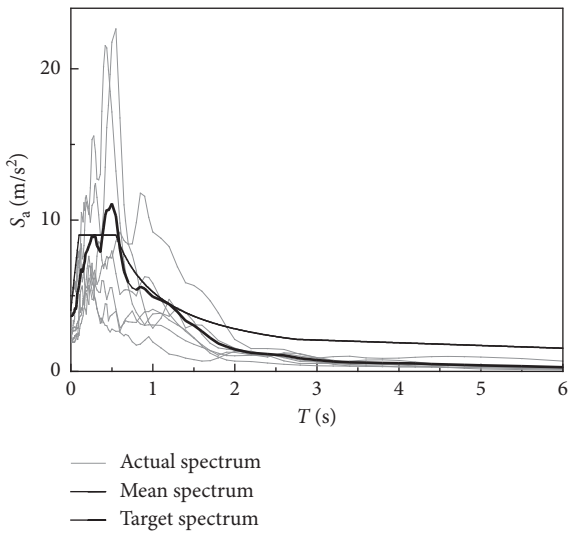

Figure 3: Acceleration spectrum of the selected ground motions.

Table 2: Parameters of near-field seismic recording.

No.	Ground motion	Magnitude	Station	Site type	Fault distance (km)	PGA (g)	PGV (cm/s)	PGV/PGA (s)
1	Imperial Valley	6.5	955 EC	C, D	4.2	0.36	76.6	0.213
2	Imperial Valley	6.5	5154ECC092	C, D	7.6	0.235	68.8	0.293
3	N. Palm Springs	6.0	5071 MV	C, D	10.1	0.205	40.9	0.204
4	Northridge	6.7	0655JFP	C, D	6.2	0.424	106.2	0.250
5	Kocaeli	7.4	Yarimca	C, D	2.6	0.268	65.7	0.245
6	Kobe	6.9	Takatori	C, D	0.3	0.611	127.1	0.208
7	Chi-Chi	7.6	CHY-101	C, D	11.14	0.44	115	0.261

Table 3: Parameters of far-field seismic recording.

No.	Ground motion	Magnitude	Station	Site type	Fault distance (km)	PGA (g)	PGV (cm/s)	PGV/PGA (s)
1	Cape Mendocino	7.1	89324RDO	C, D	18.5	0.549	42.1	0.077
2	Superstition Hills	6.7	5062SSWR	C, D	27.1	0.167	18.3	0.110
3	Coalinga	6.4	36227PC	C, D	25.5	0.227	23.6	0.104
4	Northridge	6.7	90013BH	C, D	19.6	0.516	62.8	0.208
5	Landers	7.3	22074YFS	C, D	24.9	0.152	29.7	0.195
6	Kobe	6.9	SHI090	C, D	15.5	0.212	27.9	0.132
7	San Fernando	6.6	LA-HSL	C, D	21.2	0.174	14.9	0.086

noted that the vertical component of the records are neglected according to GB50011-2010, as the total height of the model is only 23.4 m while the span length is 8 m.

It can be concluded from the comparison between the near-fault and far-fault ground motion velocity time-history curves that the structural response to the near-fault earthquake is far greater than that of the far-fault earthquake. The near-fault earthquake ground motions generate a velocity pulse with a large amplitude, a long cycle, and a short duration, whose peak amplitude region in the acceleration response spectrum is wide and generally appears in the long period section. Therefore, the IDAs of the BRBF under strong earthquakes and their aftershocks are conducted under near-fault ground motions and far-fault ground motions, respectively. The influence of the two types of ground motions is considered synthetically, and the ductility and CPD demand of the HPBRB are concluded.

4. Response of HPBRBF under a Strong Earthquake and Its Aftershocks

IDA is performed on the aforementioned six-story steel HPBRBF to obtain the performance demand of the BRBs. According to the destructive earthquakes in recent decades, strong earthquakes which may experience multiple times of strong aftershocks after the main shock frequently, in which the ground motion intensity may be lower or higher than the main shock. Though the aftershocks are never the same of the main shock, the historic records of the strong aftershocks are random. Without loss of generality, a series of continuous same record could be used to simulate the strong aftershocks or repeated earthquakes [31]. Besides, the selection of the ground motions for simulating the aftershocks could also be consulted by Hu et al. and Das et al.[32, 33]. In this paper, three continuous excitations with the same

amplitude are used as the ground motion for a single analysis to consider the effect of an earthquake and its aftershocks. During the procedure of IDA, the ground motions are scaled to different intensities to draw IDA curves. Take the near-fault ground motion of Northridge (No. 4 in Table 2), for example, the intensity of the PGA of ground motion is scaled from 1 m/s^2 to 10 m/s^2 with an interval of 1 m/s^2. The ground motion with a PGA scaled to 6 m/s^2 as an example is seen in Figure 4.

The mean interstory drift and residual drift of the HPBRBF model along the building height under the rare earthquake whose seismic precautionary intensity is 8° (i.e., PGA is 4 m/s^2) is plotted in Figure 5, in which the mean value of the responses under the near-fault ground motions and far-fault ground motions are exhibited, respectively. Meanwhile, the mean ductility demand of HPBRBs along the building height in this condition is also plotted in Figure 6, in which Figure 6(a) is the response under near-fault ground motions, while Figure 6(b) is that under the far-fault ones. It can be seen that the maximum lateral drift demand is basically concentrated on the 2nd or 3rd story of the structure, while the residual drift distribution could be seen near to zero. A similar distribution could also be seen in Figure 6. Thus, the BRBs in the 3rd story could be selected as the representative example for further analysis on the ductility demand of BRBs. Besides, it can also be seen that a relatively large drift and BRB ductility could be obtained in the top story, which is consistent with Costanzo et al. [34]. Thus, in order to improve the lateral distribution of drift demand (i.e., the ductility demand in BRBs), it can be very efficient to stiffen the top story, which could further improve the seismic performance on the chevron BRB frames.

The variation tendency of the ductility and the CPD of the HPBRB in the left side of the 3rd story with the increasing of seismic intensities in the end of different phases are presented in Figure 7.

It can be seen in Figure 7 that the ductility of the BRB almost remained the same among the three phases of excitation when the structure experiences a slight ground motion (PGA < 3 m/s^2), and the increase of the CPD after each phase is also relatively small. However, when the PGA increases to a value larger than 4 m/s^2, the ductility and the CPD of the BRB in the second phase become significantly larger than that in the first phase for the same PGA. Furthermore, the response would further increase when the third phase acts on the frame with a slight increase in amplitude. This phenomenon is more obvious with increasing PGA. According to the aforementioned phenomenon, it can be inferred that the demand of the BRB ductility under three equal-amplitude excitations is higher than that under only one. Moreover, the demand of the CPD of the BRB almost linearly increases with increasing number of the phases, implying that the accumulation of the plastic deformation caused by each phase is almost the same. It can also be concluded that higher performance requirements of the HPBRB should be proposed to achieve the target that no replacement of the HPBRB is needed during a strong earthquake and its aftershocks.

Figure 8 shows the normalized hysteretic curves of the BRBs in the third story of the HPBRBF. The two BRBs in the same story behave like an antisymmetric form, namely, the left-side BRB is mainly in compression, while the right-side BRB is mainly in tension. The gravity load of the beam-column joints may cause axial deformation of the column, resulting in a compressive stress on the BRBs before the earthquake excitation, and the compressive stress could be named as "initial stress." When the structure is subjected to ground motion, the BRB mainly in compression will yield first, while the BRB mainly in tension will yield later due to the existence of the "initial stress." As the "initial stress" caused by the gravity load of the floor exists in the BRB, the maximum pressure and the deformation of the BRB on the compression side are slightly larger than the maximum tensile force and deformation of the BRB on the tension side.

5. IDA for the Ductility

As the near-fault ground motions contain a velocity pulse that is particularly distinct compared to that for the far-fault ground motions, the ground motions for IDA in this paper are divided into two groups. The near-fault ground motion PGAs in Table 2 are scaled to a total of 10 seismic intensities (from 1 m/s^2 to 10 m/s^2) with an interval of 1 m/s^2, while the far-fault ground motion PGAs in Table 3 are scaled to a total of 12 seismic intensities (from 1 m/s^2 to 12 m/s^2) with an interval of 1 m/s^2. A set of calculations under 154 earthquake ground motions is used to generate the IDA. According to the method above, a series of data points of the engineering demand parameters μ at each PGA level under different ground motions can be obtained. The discrete data points obtained at different PGA levels in the same ground motion can be interpolated to plot the IDA curves of the BRB ductility, as shown in Figure 9.

It can be seen in Figure 9 that the response on the BRB ductility demand of the structure under the near-fault ground motions is 3~5 times larger than that under the far-fault ground motions, which indicate that the response of the long-period structure under the near-fault earthquake is relatively larger, and this phenomenon should be considered in the structural design. If the HPBRB ductility demand is determined by the response under the far-fault ground motions, the design of the HPBRB members may be partially unsafe under a near-fault ground motion. Hence, the influence of near-fault ground motion should be considered appropriately in the long-period structure and its component design.

A statistical analysis is conducted on the structural response under the two groups of ground motions, and the three quantiles of 84%, 50%, and 16% can be further obtained, in which the response of the structure under the

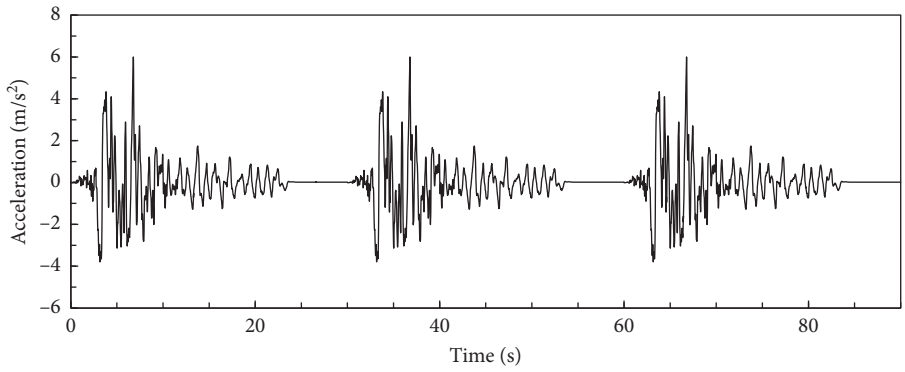

Figure 4: Seismic ground motion of Northridge.

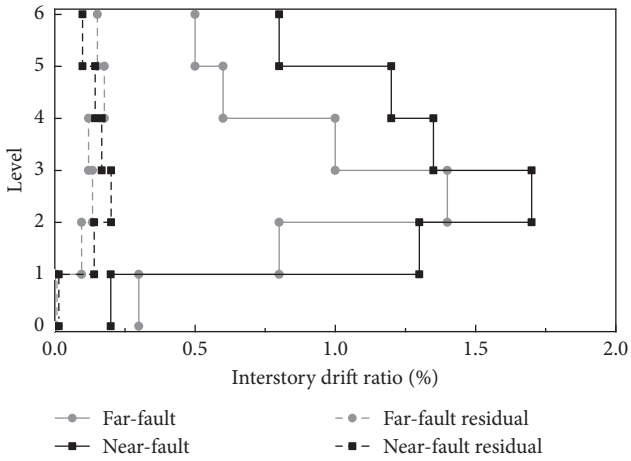

Figure 5: Interstory and residual drift ratio along the building height.

seismic motion is usually assumed to follow the lognormal distribution:

$$\Phi\left(\frac{\ln D_{84\%} - \lambda_D}{\zeta_D}\right) = 84\%,$$
$$\Phi\left(\frac{\ln D_{50\%} - \lambda_D}{\zeta_D}\right) = 50\%, \quad (4)$$
$$\Phi\left(\frac{\ln D_{16\%} - \lambda_D}{\zeta_D}\right) = 16\%,$$

where $\Phi(\cdot)$ is the cumulative distribution function of the standard normal distribution, λ_D is the logarithmic average value of D, and ζ_D is the logarithmic standard deviation of D, which is used to describe the dispersion of D. $D_{84\%}$, $D_{50\%}$, and $D_{16\%}$ expressed as follows:

$$D_{50\%} = \exp(\lambda_D),$$
$$D_{84\%} = \exp(\lambda_D + \zeta_D), \quad (5)$$
$$D_{16\%} = \exp(\lambda_D - \zeta_D).$$

The distribution curves of $D_{84\%}$, $D_{50\%}$, and $D_{16\%}$ for the ductility (μ) are shown in Figure 10.

It can be found in Figure 10 that when the seismic intensity is relatively slight (PGA < 2 m/s^2 for near-fault ground motions and PGA < 4 m/s^2 for far-fault ground motions), the discreteness of the BRB ductility is relatively small, as is the variations of the μ. However, the discreteness of the BRB ductility will arise with the increase of PGA, and this trend tends to be more obvious after PGA more than 6 m/s^2.

6. IDA for the CPD

The analysis method for the CPD of a BRB is similar to that for the BRB ductility. The discrete data points of the CPD results obtained at different PGA levels in the same ground motion can be interpolated, and the IDA curve of the BRB CPD is plotted, as shown in Figure 11.

It can be seen in Figure 11(a) that the discreteness of the response data is higher when taking the CPD as the EDP under the near-fault ground motions than that when using the ductility. This phenomenon is more significant for the far-fault ground motion, which is shown in Figure 11(b). However, the variation tendency of the CPD curve is consistent with that of the ductility curve, and the curves of $D_{84\%}$, $D_{50\%}$, and $D_{16\%}$ for CPD are shown in Figure 12.

As seen in Figure 12, when the structure is excited with a relatively slight ground motion (PGA < 2 m/s^2 for the near-fault ground motions and PGA < 4 m/s^2 for the far-fault ones), the discreteness of the CPD is small and close to zero, indicating that only part of the BRBs will yield with a small plastic strain, while other BRBs still remain elastic. However, when the PGA increased to more than 2 m/s^2, the discreteness of the BRB CPD increases, and the amplitude can be seen more obvious with increasing PGA. Furthermore, this tendency is much more obvious in the statistical distribution curve of the far-fault seismic response. This is because the BRB CPD is related to not only the BRB maximum strain but also to the cyclic number of the BRBs. Due to the differences among the various ground motions, when the frame was considered under the aftershocks, the residual deformation of the frame in each earthquake excitation will affect the statistical results of the CPD.

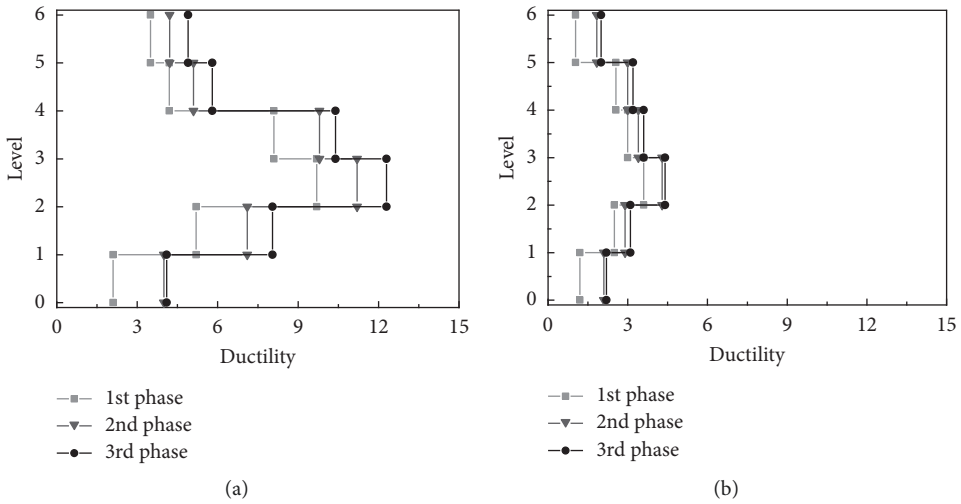

Figure 6: Ductility distribution of HPBRBs along the building height: (a) near-fault condition; (b) far-fault condition.

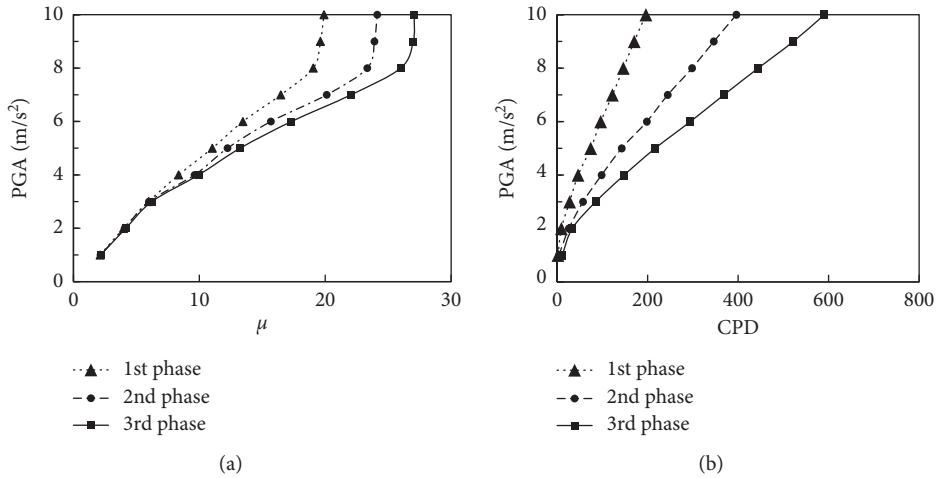

Figure 7: Comparison of the three seismic response of a BRB: (a) PGA-ductility; (b) PGA-CPD.

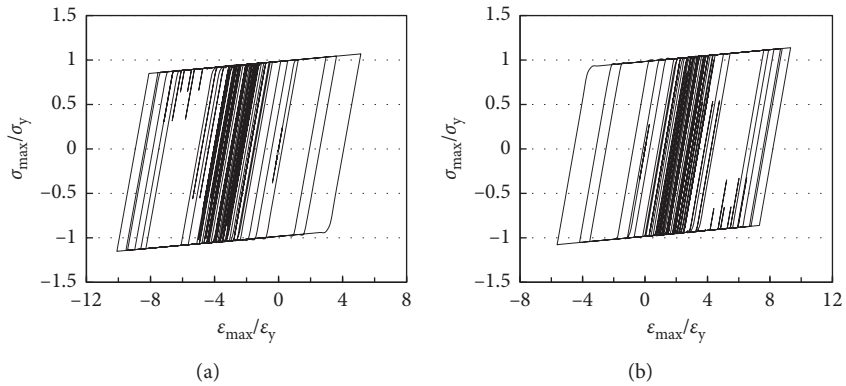

Figure 8: Hysteretic curves of BRBs on the third floor: (a) BRB on the left; (b) BRB on the right.

7. PSHC of the PGA

As the probability of the PGA exceeding a given value A is defined in a 50-year period according to the Seismic Ground Motion Parameter Zonation Map of China (GB18306-2001) [35] in China, it is assumed that the probability distribution of the PGA conforms to the extreme-II distribution, and the probability of the PGA exceeding the value A in 50 years is

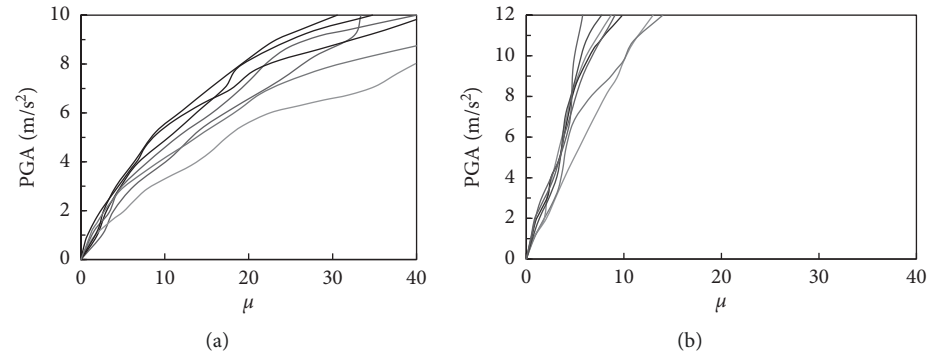

Figure 9: IDA curves of the BRB ductility: (a) response to near-fault ground motion; (b) response to far-fault ground motion.

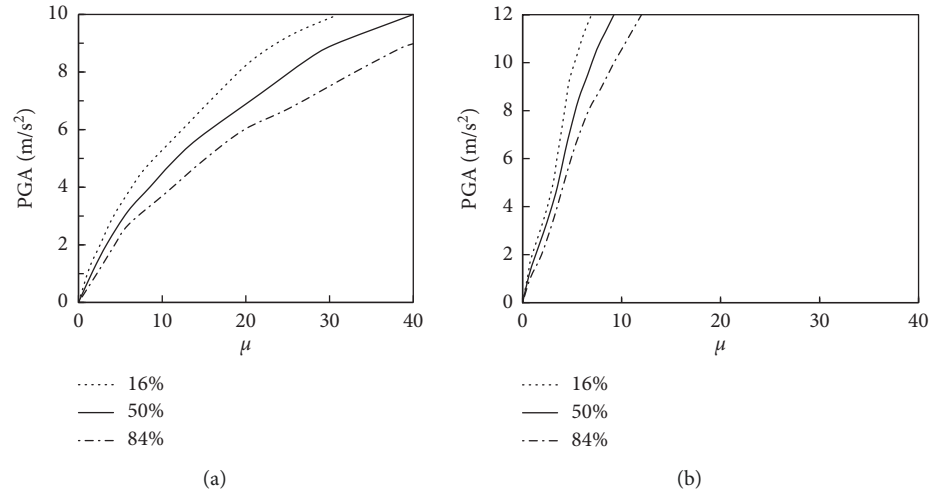

Figure 10: Distribution statistics of BRB ductility: (a) response to near-fault ground motion; (b) response to far-fault ground motion.

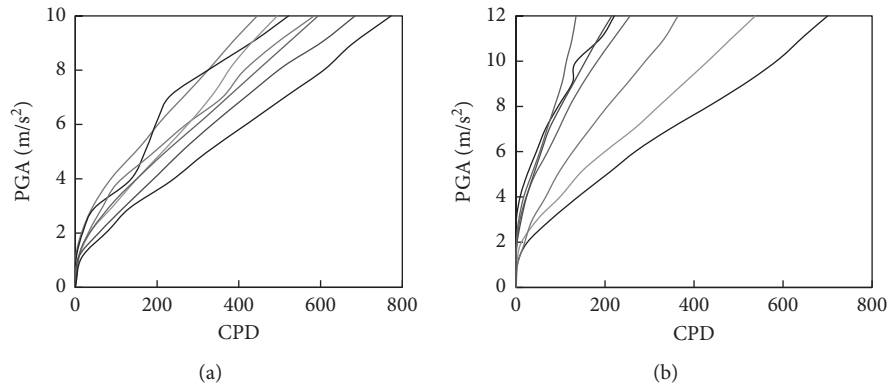

Figure 11: IDA curves of the CPD of a BRB: (a) response to near-fault ground motion; (b) response to far-fault ground motion.

$$\lambda_{\mathrm{PGA}}(A) = 1 - F_{\mathrm{II}}(A) = 1 - \exp\left[-\left(\frac{A}{A_{\mathrm{g}}}\right)^{-k}\right], \quad (6)$$

where A_{g} is the PGA whose exceedance probability is 63.2% in 50 years and k is a shape factor of the distribution of the ground motion.

According to the statistical result of Gao and Bao [36], k and A_{g} are 2.35 and $0.385A_{10}$, respectively, in which A_{10} is the PGA whose exceedance probability in 50 years is 10%, namely, the design basic acceleration in Chinese Code [22], and A_{10} is 2 m/s^2, as suggested by the code in which the seismic fortification intensity is 8°. The character of the site belongs to Type III, and the design characteristic period of

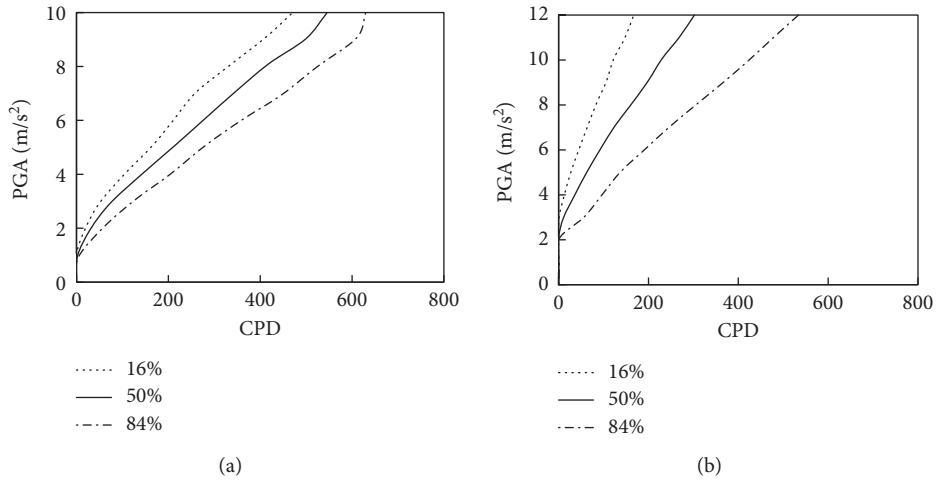

Figure 12: Distribution statistics of the BRB CPD: (a) response to near-fault ground motion; (b) response to far-fault ground motion.

ground motion belongs to the first group. Eq. (6) can then be expressed as

$$\lambda_{\mathrm{PGA}}(A) = 1 - F_{\mathrm{II}}(A) = 1 - \exp\left(-0.516A^{-2.35}\right). \quad (7)$$

The probability of the PGA exceeding the value A in 50 years can be obtained by Eq. (7), and the PSHC of the PGA of the model in this paper is expressed in Figure 13.

The probability density function curve of the PGA exceeding a determined value A in 50 years can be obtained by taking the derivative of Eq. (7), which is expressed as Eq. (8) and shown in Figure 14:

$$\frac{d\lambda_{\mathrm{PGA}}(A)}{dA} = 0.626A^{-5.7} \cdot \exp\left(-0.516A^{-2.35}\right). \quad (8)$$

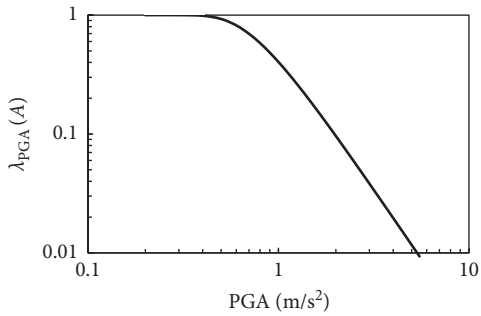

Figure 13: PSHC of the PGA.

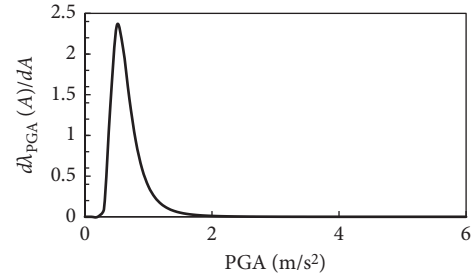

Figure 14: Probability distribution of PGA.

8. Seismic Demand Analysis of HPBRB

8.1. Probabilistic Seismic Demand Curves. According to the aforementioned analysis, when the EDP is assumed to obey the lognormal distribution, the logarithmic standard deviation of the EDP is a variable for the different amplitudes of ground motions. To fully consider the discreteness of the ground motions, the numerical method is used to solve Eq. (2), whose basic idea is to divide the whole integral interval $[A_{\min}, A_{\max}]$ into several subintervals $[A_i, A_{i+1}]$, $i = 1, 2, \ldots, n$, in which $A_1 = A_{\min}$ and $A_{n+1} = A_{\max}$ and $n = 600$ in this example. Eq. (2) can be further expressed as

$$\lambda_{\mathrm{EDP}}\left(\delta_j\right) = \sum_{i=1}^{n} P\left[\mathrm{EDP} > \delta_j \mid \mathrm{PGA} = A_i\right] \cdot \left.\frac{d\lambda_{\mathrm{PGA}}(A)}{dA}\right|_{A_i} \cdot \Delta A_i, \quad (9)$$

where $\Delta A_i = A_{i+1} - A_i$.

The specific steps are as follows:

(1) Select an EDP value δ_j and choose the integral range of the PGA as [0, 6] m/s^2 and divide the PGA range into identical 600 parts

(2) Conduct an interpolation of the quantile curves according to the statistical results of the IDA curves and obtain the corresponding EDP logarithmic mean value λ_i and the logarithmic standard deviation ζ_i in each interval A_i ($i = 1, 2, \ldots, 600$)

(3) Calculate the conditional probability of $\mathrm{EDP} > \delta_j$ under the given $\mathrm{PGA} = A_i$ with the assumption that the EDP obeys the lognormal distribution:

$$P\left[\mathrm{EDP} > \delta_j \mid \mathrm{PGA} = A_i\right] = 1 - P\left[\mathrm{EDP} \le \delta_j \mid \mathrm{PGA} = A_i\right] = 1 - \Phi\left(\frac{\ln \delta_j - \lambda_i}{\zeta_i}\right), \quad (10)$$

where $\Phi(\cdot)$ is the standard normal distribution function

(4) Obtain the probability of EDP $> \delta_j$ in 50 years considering the probability that the PGA is around the value A_i, which is the product of the shaded areas shown in Figures 15(a) and 15(b)

(5) Repeat steps (3) and (4) for different A_i and summarize the results to obtain the probability that EDP $> \delta_j$ in 50 years, $\lambda_{\mathrm{EDP}}(\delta_j)$

(6) Repeat steps (1) to (5) for another EDP $= \delta_j$ and fit the series of discrete data points and draw the PSDC

9. PSDC of HPBRB Ductility

The exceedance probability of the BRB ductility demand in 50 years under the two types of ground motion analyses is shown in Figure 16.

Combined with the PSHC, the HPBRB ductility demand for a determined exceedance probability, which is demanded for an HPBRBF under a strong earthquake and its aftershocks within the 50-year design reference period, can be determined. As is analyzed in Section 3, the theoretical value obtained from this section should be multiplied by 2 to obtain the true HPBRB ductility demand of the actual structure.

It can be seen in Figure 16 that the HPBRB ductility demand of μ is 13.4 for the near-fault ground motions under the condition that the exceedance probability of the BRB ductility demand in 50 years is 5%, while 25.7 for 2% and 33 for 1%. However, the ductility demand for the far-fault ground motion group is 5.8, 9.1, and 11.4, respectively, for the condition in which the exceedance probability is 5%, 2%, and 1%. It can be seen that the HPBRB ductility demand for the near-fault ground motion is much larger than that for the far-fault ground motion, and the former is nearly three times than that of the latter.

10. PSDC of HPBRB CPD

It can be determined from Figure 17 that the HPBRB CPD demand is 190 for the near-fault ground motions as the exceedance probability in 50 years is 5%, while CPD demand of 310 and 640 are needed under the condition that the exceedance probability is 2% and 1%, respectively. However, the CPD demand for the far-fault ground motion group is 60, 100, and 180, respectively, as the exceedance probability in 50 years is 5%, 2%, and 1%. It can also be seen that the HPBRB CPD demand for the near-fault ground motion is much larger than that for the far-fault ground motion, and the former is nearly three times than that of the latter.

The limit value for CPD demand of 200 suggested by ANSI/AISC [11] seems to be reasonable for the condition of the far-fault ground motions, but it may be excessively low for the near-fault strong ground motions. The HPBRB CPD demand with 98% assurance rate is much larger than the limit value of the AISC, and the demand with 99% assurance rate is more than twice than that of the AISC limit, which indicates that the CPD demand for the HPBRB is expected to be higher in order to ensure a high low-cycle fatigue capacity for the HPBRB under the excitation of a strong earthquake and its aftershocks. Since a significant randomness on the CPD of HPBRBs is existed, the minimum threshold of the CPD demand should be determined. Furthermore, it is necessary to put forward a stricter minimum threshold value in order to satisfy the demand for HPBRBs.

In conclusion, the ductility and CPD demand of the HPBRB in the frame under different exceedance probabilities are listed in Table 4. It is suggested that the design demand for ductility and CPD of HPBRBs should follow the condition that the exceedance probability is 1%.

11. Conclusions

The analyses of the ductility and CPD demand of an HPBRB under a strong earthquake and its aftershocks are conducted in this paper. A six-story BRBF is taken as an example, a near-fault ground motion Northridge is selected to conduct the IDA on the BRBF. The seismic responses of the BRBF under one, two, and three constant continuous ground motions are compared. The IDA result indicates that the ductility and CPD demand of the BRBs under the three constant continuous ground motions are significantly larger than that excited by only one ground motion. This trend becomes more significant with increasing PGA of the ground motion. The CPD demand for three earthquakes is nearly 3 times than that for only one earthquake when the PGA is larger than 2 m/s^2. The analysis result indicates that it is essential to conduct research on the EDP demand of HPBRBs under strong earthquakes and continuous strong aftershocks.

Seven near-fault ground motions and seven far-fault ground motions are selected to consider the indeterminacy of ground motion, and the PGA ranges from 1 m/s^2 to 10 m/s^2 (1 m/s^2 to 12 m/s^2 for the far-fault motions). A total of 154 ground motions are used to excite the BRBFs, and the IDA curves are obtained by statistics. Probability seismic hazard analysis (PSHA) is performed to obtain the PSHC for the PGA. Then, the PSDCs for the ductility and CPD demand for the HPBRB under three constant continuous strong earthquakes are obtained through PSDA. These curves indicate that the ductility demand and CPD demand for the HPBRB under the near-fault ground motions are much larger than those under the far-fault ground motions, and the CPD demand under the near-fault ground motions is approximately three times larger than that under the far-fault ones. The analysis results indicate that the ductility demand for the HPBRB under the near-fault earthquake condition is 25.7 when the exceedance probability in 50 years is 2%, while it is 33 when the exceedance probability in 50 years is strictly controlled to 1%; the CPD demand is 310 and 640, respectively, for the exceedance probability 2% and 1% in 50 years. If the design does not require the consideration of the effect of near-fault earthquakes, the demand of the ductility and CPD of a BRB can be properly relaxed at 11.4 and 180, respectively, for the exceedance probability in 50 years is 1%. It is seen in the AISC that the minimum threshold of the CPD of BRBs is 200, which may be reasonable for the structures under the

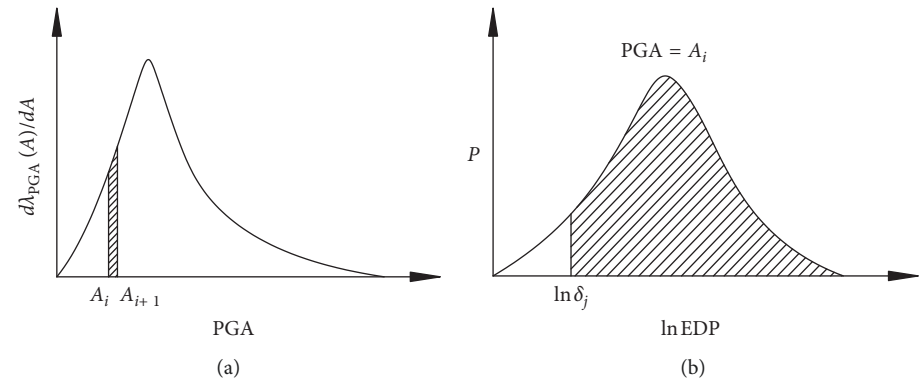

Figure 15: (a) Probability distribution of PGA and (b) probability distribution of EDP under PGA = A_i.

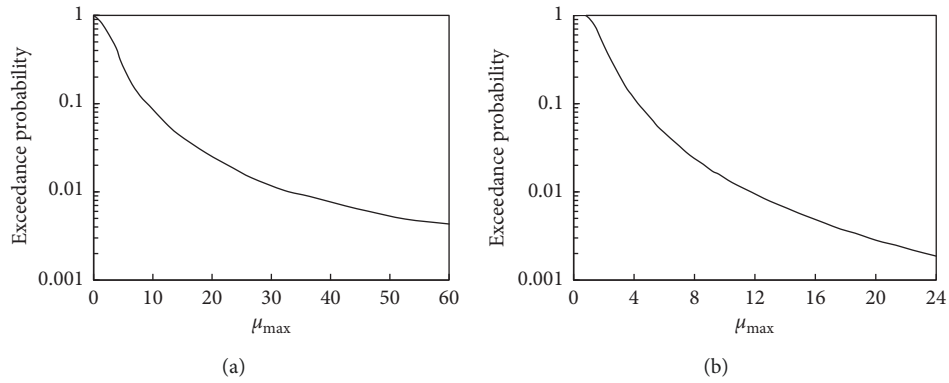

Figure 16: PSDC of the HPBRB ductility: (a) near-fault ground motion group; (b) far-fault ground motion group.

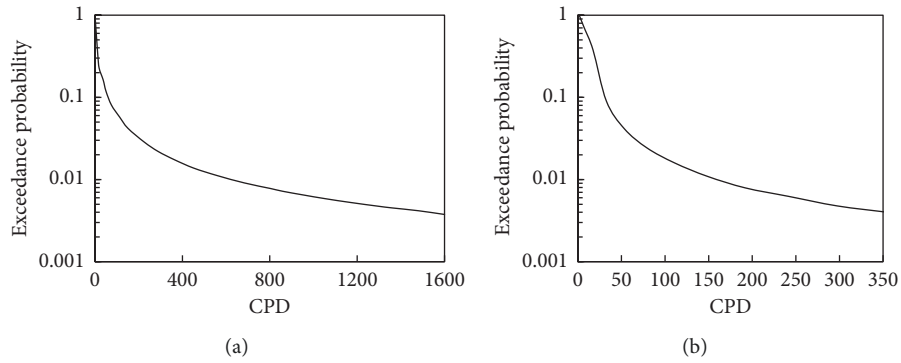

Figure 17: PSDCs of the BRB CPD: (a) near-fault ground motion group; (b) far-fault ground motion group.

Table 4: Ductility and CPD demand of an HPBRB.

Exceedance probability (%)	EDP			
	μ		CPD	
	Near-fault	Far-fault	Near-fault	Far-fault
5	13.4	5.8	190	60
2	25.7	9.1	310	100
1	33.0	11.4	640	180

far-fault ground motion; however, this value is excessively low for the condition of continuous strong aftershocks of near-fault excitations. Furthermore, as there is a large randomness on the CPD capacity of HPBRBs, this paper suggests that the minimum threshold of the CPD demand should be determined by a low exceedance probability.

Data Availability

The data used to support the findings of this study are included within the article.

Conflicts of Interest

The authors declare that there are no conflicts of interest regarding the publication of this paper.

Acknowledgments

The authors would like to acknowledge financial support from the China National Key Research and Development Program (2016YFC0701403), the National Natural Science Foundation of China (51278105), and the Priority Academic Program Development of Jiangsu Higher Education Institutions (PAPD).

References

[1] G. Della Corte, M. D'Aniello, R. Landolfo, and F. M. Mazzolani, "Review of steel buckling-restrained braces," *Steel Construction*, vol. 4, no. 2, pp. 85–93, 2011.

[2] L. Di Sarno and G. Manfredi, "Experimental tests on full-scale RC unretrofitted frame and retrofitted with buckling-restrained braces," *Earthquake Engineering & Structural Dynamics*, vol. 41, no. 2, pp. 315–333, 2011.

[3] T. Usami, T. Sato, and A. Kasai, "Developing high-performance buck-ling-restrained braces," *Journal of structural engineering (JSCE)*, vol. 55A, pp. 719–729, 2009, in Japanese.

[4] C.-L. Wang, T. Usami, and J. Funayama, "Improving low-cycle fatigue performance of high-performance buckling-restrained braces by toe-finished method," *Journal of Earthquake Engineering*, vol. 16, no. 8, pp. 1248–1268, 2012.

[5] FEMA-450, *NEHRP Recommended Provisions for Seismic Regulations for New Buildings and Other Structures*, Federal Emergency Management Agency, Washington, DC, USA, 2003.

[6] R. Sabelli, *Research on Improving the Design and Analysis of Earthquake-Resistant Steel-Braced Frames*, EERI, Oakland, CA, USA, 2001.

[7] M. Iwata, T. Kato, and A. Wada, "Performance evaluation of buckling-restrained braces in damage-controlled structures," in *Behavior of Steel Structures in Seismic Areas*, pp. 37–43, STESSA, San Francisco, CA, USA, 2003.

[8] T. Usami, A. Kasai, and M. Kato, "Behavior of buckling-restrained brace members," in *Proceedings of 4th International Conference on STESSA 2003-Behavior of Steel Structures in Seismic Areas*, pp. 211–216, Naples, Italy, June 2003.

[9] ANSI/AISC 360-10, *Seismic Provisions of Structural Steel Buildings*, American Institute of Steel Construction, Chicago, IL, USA, 2010.

[10] L. Di Sarno, "Effects of multiple earthquakes on inelastic structural response," *Engineering Structures*, vol. 56, pp. 673–681, 2013.

[11] T. Usami, "Developing high-performance damage control seismic dampers," in *Proceedings of the 10th Symposium on Ductile Design Method for Bridges (Special Lecture)*, pp. 11–22, Tokyo, Japan, 2007.

[12] M. Jia, X. Yu, D. Lu, and B. Lu, "Experimental research of assembled buckling-restrained braces wrapped with carbon or basalt fiber," *Journal of Constructional Steel Research*, vol. 131, pp. 144–161, 2017.

[13] L.-J. Jia, H. Ge, R. Maruyama, and K. Shinohara, "Development of a novel high-performance all-steel fish-bone shaped buckling-restrained brace," *Engineering Structures*, vol. 138, pp. 105–119, 2017.

[14] C.-L. Wang, Q. Chen, B. Zeng, and S. Meng, "A novel brace with partial buckling restraint: an experimental and numerical investigation," *Engineering Structures*, vol. 150, pp. 190–202, 2017.

[15] Q. Chen, C.-L. Wang, S. Meng, and B. Zeng, "Effect of the unbonding materials on the mechanic behavior of all-steel buckling-restrained braces," *Engineering Structures*, vol. 111, pp. 478–493, 2016.

[16] Y.-L. Guo, J.-S. Zhu, P. Zhou, and B.-L. Zhu, "A new shuttle-shaped buckling-restrained brace. Theoretical study on buckling behavior and load resistance," *Engineering Structures*, vol. 147, pp. 223–241, 2017.

[17] Y.-L. Guo, P.-P. Fu, P. Zhou, and J.-Z. Tong, "Elastic buckling and load resistance of a single cross-arm pre-tensioned cable stayed buckling-restrained brace," *Engineering Structures*, vol. 126, pp. 516–530, 2016.

[18] Y.-L. Guo, P. Zhou, M. Andrew Bradford, Y.-L. Pi, J.-Z. Tong, and P.-P. Fu, "Theoretical and numerical studies of elastic buckling and load resistance of double cross-arm pre-tensioned cable stayed buckling-restrained braces," *Engineering Structures*, vol. 153, pp. 674–699, 2017.

[19] B.-L. Zhu, Y.-L. Guo, P. Zhou, M. A. Bradford, and Y.-L. Pi, "Numerical and experimental studies of corrugated-web-connected buckling-restrained braces," *Engineering Structures*, vol. 134, pp. 107–124, 2017.

[20] L. Xie, J. Wu, and Q. Huang, "Experimental study on low-cycle fatigue performance of weld-free buckling-restrained braces," *Journal of Earthquake Engineering*, vol. 22, no. 8, pp. 1392–1414, 2018.

[21] N. Hoveidae, R. Tremblay, B. Rafezy, and A. Davaran, "Numerical investigation of seismic behavior of short-core all-steel buckling restrained braces," *Journal of Constructional Steel Research*, vol. 114, pp. 89–99, 2015.

[22] D. Vafaei and R. Eskandari, "Seismic response of mega buckling-restrained braces subjected to fling-step and forward-directivity near-fault ground motions," *Structural Design of Tall and Special Buildings*, vol. 24, no. 9, pp. 672–686, 2014.

[23] D. Vamvatsikos and C. A. Cornell, "Incremental dynamic analysis," *Earthquake Engineering & Structural Dynamics*, vol. 31, no. 3, pp. 491–514, 2002.

[24] P. Tothong and N. Luco, "Probabilistic seismic demand analysis using advanced ground motion intensity measures," *Earthquake Engineering & Structural Dynamics*, vol. 36, no. 13, pp. 1837–1860, 2007.

[25] Y. Ding and Y. Zhang, "Design and seismic response of tall chevron panel buckling-restrained braced steel frames," *Structural Design of Tall and Special Buildings*, vol. 22, no. 14, pp. 1083–1104, 2011.

[26] GB 50011-2010, *Code for Seismic Design of Buildings*, Ministry of Housing and Urban-Rural Development of the People's Republic of China, Beijing, China, 2010, in Chinese.
[27] S. SeismoSoft, "A computer program for static and dynamic nonlinear analysis of framed structures," 2016, http://www.seismosoft.com.
[28] T. Usami, Z. Lu, and H. Ge, "A seismic upgrading method for steel arch bridges using buckling-restrained braces," *Earthquake Engineering & Structural Dynamics*, vol. 34, no. 45, pp. 471–496, 2005.
[29] E. Kalkan and S. K. Kunnath, "Effects of fling step and forward directivity on seismic response of buildings," *Earthquake Spectra*, vol. 22, no. 2, pp. 367–390, 2006.
[30] N. Jayaram, T. Lin, and J. W. Baker, "A computationally efficient ground-motion selection algorithm for matching a target response spectrum mean and variance," *Earthquake Spectra*, vol. 27, no. 3, pp. 797–815, 2011.
[31] X. Chen, H. Ge, and T. Usami, "Seismic demand of buckling-restrained braces installed in steel arch bridges under repeated earthquakes," *Journal of Earthquake and Tsunami*, vol. 5, no. 2, pp. 119–150, 2011.
[32] S. Hu, P. Gardoni, and L. Xu, "Stochastic procedure for the simulation of synthetic main shock-aftershock ground motion sequences," *Earthquake Engineering & Structural Dynamics*, vol. 47, no. 11, pp. 2275–2296, 2018.
[33] S. Das and V. K. Gupta, "Wavelet-based simulation of spectrum-compatible aftershock accelerograms," *Earthquake Engineering & Structural Dynamics*, vol. 37, no. 11, pp. 1333–1348, 2008.
[34] S. Costanzo, M. D'Aniello, and R. Landolfo, "Seismic design criteria for chevron CBFs: proposals for the next EC8 (part-2)," *Journal of Constructional Steel Research*, vol. 138, pp. 17–37, 2017.
[35] GB18306-2001, *Seismic Ground Motion Parameter Zonation Map of China*, Bureau of Quality and Technical Supervision of the People's Republic of China, Beijing, China, 2001, in Chinese.
[36] X. W. Gao and A. B. Bao, "Probabilistic model and its statistical parameters for seismic load," *Earthquake Engineering and Engineering Vibration*, vol. 5, no. 1, pp. 13–22, 1985, in Chinese.